Current Biology 16, 755–766, April 18, 2006 ©2006 Elsevier Ltd All rights reserved DOI 10.1016/j.cub.2006.03.057

Article

In Vitro FRAP Identifies the Minimal Requirements for Mad2 Kinetochore Dynamics

Martin Vink,[1] Marco Simonetta,[1] Pietro Transidico,[2] Karin Ferrari,[1] Marina Mapelli,[1,2] Anna De Antoni,[1] Lucia Massimiliano,[1,2] Andrea Ciliberto,[2] Mario Faretta,[1,2] Edward D. Salmon,[3] and Andrea Musacchio[1,2,*]

[1] Department of Experimental Oncology
European Institute of Oncology
Via Ripamonti 435
20141 Milan
Italy

[2] FIRC Institute of Molecular Oncology Foundation
Via Adamello 16
20139 Milan
Italy

[3] Department of Biology
University of North Carolina at Chapel Hill
607 Fordham Hall
Chapel Hill, North Carolina 27599

Summary

Background: Mad1 and Mad2 are constituents of the spindle-assembly checkpoint, a device coupling the loss of sister-chromatid cohesion at anaphase to the completion of microtubule attachment of the sister chromatids at metaphase. Fluorescence recovery after photobleaching (FRAP) revealed that the interaction of cytosolic Mad2 with kinetochores is highly dynamic, suggesting a mechanism of catalytic activation of Mad2 at kinetochores followed by its release in a complex with Cdc20. The recruitment of cytosolic Mad2 to kinetochores has been attributed to a stable receptor composed of a distinct pool of Mad2 tightly bound to Mad1. Whether specifically this interaction accounts for the kinetochore dynamics of Mad2 is currently unknown.

Results: To gain a precise molecular understanding of the interaction of Mad2 with kinetochores, we reconstituted the putative Mad2 kinetochore receptor and developed a kinetochore recruitment assay with purified components. When analyzed by FRAP in vitro, this system faithfully reproduced the previously described in vivo dynamics of Mad2, providing an unequivocal molecular account of the interaction of Mad2 with kinetochores. Using the same approach, we dissected the mechanism of action of $p31^{comet}$, a spindle-assembly checkpoint inhibitor.

Conclusions: In vitro FRAP is a widely applicable approach to dissecting the molecular bases of the interaction of a macromolecule with an insoluble cellular scaffold. The combination of in vitro fluorescence recovery after photobleaching with additional fluorescence-based assays in vitro can be used to unveil mechanism, stoichiometry, and kinetic parameters of a macromolecular interaction, all of which are important for modeling protein interaction networks.

*Correspondence: andrea.musacchio@ifom-ieo-campus.it

Introduction

Fluorescence recovery after photobleaching (FRAP) is an imaging technique that takes advantage of the fact that fluorophores can be irreversibly photobleached within a given area by using a focused beam of light [1, 2]. If biological molecules containing bleached fluorophores leave the area, they will be replaced with nonbleached fluorescent molecules. This allows kinetics measurements and the determination of the fraction of recovery, which can reveal the existence of a spatially fixed, immobile fraction of the ligand that cannot be replaced with ligand bound to unbleached fluorophores from solution [1, 2].

Among FRAP's several insightful applications is the possibility of studying the kinetics of binding of macromolecules to various cellular compartments and organelles [1, 2]. A limitation of these studies, however, is that the relationship between the kinetic FRAP measurements and the specific molecular interactions on which they are based usually remains unknown. This is because in most cases the identity of the macromolecules involved and their regulation are not known in sufficient detail. A possible strategy to overcome this limitation consists in (1) making an assumption about the identity of the molecular players in the interaction, (2) reconstituting the interaction in vitro with purified components, (3) measuring the dynamic properties of this reconstituted system, and (4) assessing their similarity with values determined in vivo [2]. Arguably, this approach would have widespread beneficial consequences on our ability to model complex biological systems [3, 4].

Here, we provide an account of our attempts to apply this strategy to the study of the interaction of the spindle-assembly checkpoint (SAC) protein Mad2 with kinetochores, because this has been extensively investigated by FRAP in vivo [5–8]. Kinetochores are complex protein scaffolds that assemble on centromeric DNA. They mediate the attachment of microtubules during mitosis and recruit the SAC proteins to monitor this process [9]. For coordinating the onset of anaphase with the completion of the attachment process, Mad2 is believed to be activated at unattached kinetochores to sequester Cdc20, its target in the checkpoint [10, 11]. Mad2 has two stable conformations differing for the position of a 50 residue segment at its C terminus [12, 13]. The closed conformation (C-Mad2) is observed when Mad2 binds Cdc20 [12, 13]. C-Mad2 is also observed in the complex of Mad2 with Mad1, a SAC protein that is necessary for Mad2 kinetochore recruitment [13–18]. The open conformation of Mad2 (O-Mad2) is the physiological state of cytosolic Mad2 in the absence of Mad1 or Cdc20 [19, 20].

As summarized in Table 1A–1E, FRAP experiments on Mad2 provided apparently conflicting results. Two studies (Table 1B and 1C) using either transient transfection

Table 1. Kinetic Analyses

Row	Method	Support	Receptor*	Ligand*	Ligand concentration	k_{on} ($M^{-1}s^{-1}$)	k_{off} (s^{-1})	Half-time (s)	Percent Recovery (%)	N	p value[a]	Comments and Reference
Studies in vivo												
A	FRAP	Unattached Kinetochores	Mad1:C-Mad2 (hypothetical)	YFP-$Mad2^{wt}$ $Mad2^{wt}$-YFP	Unknown	NA	0.11–0.06	6.4–10.8	~50	See [7]	Unk	Stable Expression [7]
B	FRAP	Unattached Kinetochores	Mad1:C-Mad2 (hypothetical)	Alexa488-$Mad2^{wt}$	Unknown	NA	0.027	26	84 ± 23	See [6]	Unk	Protein injection [6]
C	FRAP	Unattached Kinetochores	Mad1:C-Mad2 (hypothetical)	GFP-$Mad2^{wt}$	Unknown	NA	0.036	19	91 ± 17	See [5]	Unk	Transient expression [5]
D	FRAP	Unattached Kinetochores	Mad1:C-Mad2 (hypothetical)	Alexa488-$Mad2^{wt}$	Unknown	NA	0.027 ± 0.014	25.1 ± 10.1	85 ± 16	8	NA	Protein injection This study
E	FRAP	Unattached Kinetochores	Mad1:C-Mad2 (hypothetical)	Alexa488-$Mad2^{\Delta C}$	Unknown	NA	0.034 ± 0.035	20.3 ± 9.7	80 ± 17	12	0.29[b]	Protein injection This study
Studies *in vitro*												
F	FRAP	Beads	Mad1-bound CFP-C-Mad2	CFP-$Mad2^{wt}$	15 μM	NA	0.186 ± 0.066	4.2 ± 1.6	38 ± 5	17	0.687[c]	This study
G	FRAP	Beads	Mad1-bound unlabeled C-Mad2	CFP-$Mad2^{wt}$	15 μM	NA	0.191 ± 0.049	3.9 ± 1.1	87 ± 8	72	NA	This study
H	FRAP	Beads	Mad1 immunoprecipitate	CFP-$Mad2^{wt}$	15 μM	NA	0.214 ± 0.062	3.5 ± 1.1	75 ± 8	5	0.329[c]	This study
I	FRAP	Beads	Mad1-bound unlabeled C-Mad2	Alexa488-$Mad2^{wt}$	15 μM	NA	0.195 ± 0.034	3.7 ± 0.6	78 ± 9	42	0.682[c]	This study
J	FRAP	Beads	Mad1-bound unlabeled C-Mad2	CFP-$Mad2^{\Delta C}$	15 μM	NA	0.387 ± 0.078	1.9 ± 0.3	89 ± 12	15	< 0.01[c]	This study
K	FRAP	Beads	Mad1-bound unlabeled C-Mad2	Alexa488-$Mad2^{\Delta C}$	15 μM	NA	0.430 ± 0.122	1.7 ± 0.5	76 ± 9	46	< 0.01[c]	This study
L	FRAP	Beads	Mad1-bound unlabeled C-Mad2	CFP-$p31^{comet}$	8 μM	NA	0.037 ± 0.08	19.7 ± 4.1	88 ± 8	13	NA	This study
M	Sequential FRAP	Beads	1st round Mad1-bound CFP-C-Mad2	CFP-$Mad2^{wt}$	15 μM	NA	1st round See row F	1st round See row F	1st round See row F	1st round See row F	1st round See row F	This study
M	Sequential FRAP	Beads	2nd round Mad1-bound bleached CFP-C-Mad2	CFP-$Mad2^{wt}$	15 μM	NA	2nd round 0.175 ± 0.070	2nd round 4.6 ± 1.7	2nd round 75 ± 5	2nd round 12	2nd round 0.333[c]	This study
N	FRAP	Flat substrate	Mad1-bound unlabeled C-Mad2	CFP-$Mad2^{wt}$	2 μM	NA	0.230 ± 0.001	3.0 ± 0.0	79 ± 5	5	0.087[c]	This study
O	Off rate	Flat substrate	Mad1-bound Unlabeled C-Mad2	CFP-$Mad2^{wt}$ + Unlabeled $Mad2^{wt}$	2 μM 40 μM	NA	0.139 ± 0.007	4.9 ± 0.27	NA	5	NA	This study
P	Off rate	Flat substrate	Mad1-bound Unlabeled C-Mad2	CFP-$Mad2^{wt}$ + Unlabeled $Mad2^{\Delta C}$	2 μM 40 μM	NA	0.140 ± 0.004	4.9 ± 0.14	NA	5	0.87[d]	This study
Q	Off rate	Flat substrate	Mad1-bound Unlabeled C-Mad2	CFP-$Mad2^{wt}$ + Unlabeled $Mad2^{\Delta C}$ + $Cdc20^{111–138}$	2 μM 40 μM 40 μM	NA	0.141 ± 0.003	4.9 ± 0.10	NA	5	0.59[d]	This study
R	Calculation (K_D and k_{off})	NA	Mad1-bound Unlabeled C-Mad2	CFP-Mad2	NA	$2 \cdot 10^5$	As in row F	As in row F	As in row F	NA	NA	This study
S	Calculation (K_D and k_{off})	NA	Mad1-bound unlabeled C-Mad2	CFP-$p31^{comet}$	NA	$1.7 \cdot 10^6$	As in row K	As in row K	As in row K	NA	NA	This study

NA denotes not applicable, and ITC denotes Isothermal Titration Calorimetry. *Indicates that human sequences were used throughout.

[a] p value: Student's t based on comparison of rate constants.

[b] p value relative to experiment in row D.

[c] p value relative to experiment in row G.

[d] p value relative to experiment in row O.

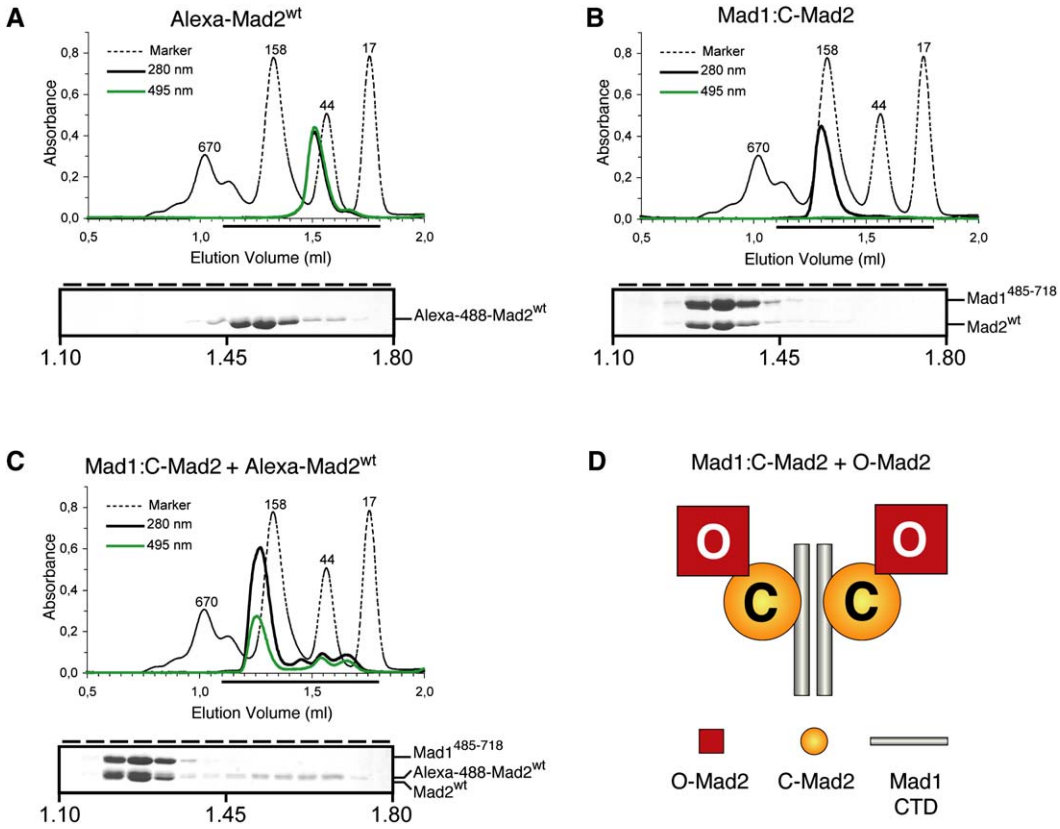

Figure 1. Mad2 and Its Biochemistry

(A) Elution profile of Alexa-Mad2^{wt} from a Superdex 200 PC 3.2/30 size-exclusion chromatography (SEC) column. SDS-PAGE and Coomassie staining of the content of fourteen 50 μl fractions eluting between 1.10 and 1.80 ml are shown. Traces were recorded at 280 nm and 495 nm are black and green, respectively.

(B) Profile of unlabeled Mad1:Mad2. Absorbance at 495 nm was not observed because the complex is unlabeled.

(C) Alexa-Mad2^{wt} was mixed with stoichiometric amounts of unlabeled Mad1:Mad2 and incubated for 1 hr prior to SEC. Most Alexa-Mad2 signal eluted with the Mad1:Mad2 complex, which was shifted toward higher molecular weights upon binding Alexa-Mad2.

(D) Schematic representation of the interaction of O-Mad2 (red square) with C-Mad2 bound to the C-terminal domain of Mad1 (yellow circles and gray rectangle, respectively).

of GFP-Mad2 or direct injection of Alexa-fluor-488-labeled Mad2 in live cells prior to mitosis reported near to 100% recovery of Mad2 kinetochore fluorescence [5, 6]. Another study (Table 1A) exploiting stable cell lines expressing YFP-Mad2 revealed instead that the rapidly exchanging pool of Mad2 accounts for ~50% of kinetochore Mad2, whereas another ~50% resides stably at these structures [7]. All studies, on the other hand, found that Mad1 is mainly a stable kinetochore resident in mitosis [5, 7]. These observations led to the hypothesis that a complex of Mad1 with Mad2 (Mad1:Mad2), accounting for the immobile Mad1 and Mad2 fractions, might be responsible for the recruitment of a mobile fraction of Mad2 from the cytosol [7]. The "Mad2 template" hypothesis [19] tried to provide a more detailed molecular description of this reaction by proposing that the cytosolic fraction of Mad2, which adopts the O-Mad2 conformation, is recruited to the kinetochores by the C-Mad2 conformer in the Mad1:C-Mad2 complex. According to the "Mad2 template" model, the ability of O-Mad2 to form a conformational dimer with C-Mad2 is the critical interaction for kinetochore recruitment of cytosolic O-Mad2. The significance of the model will be discussed thoroughly later in this paper.

We reasoned that if the molecular description of the Mad2 kinetochore cycle provided by the "Mad2 template" model were correct, a system of purified components and defined composition containing O-Mad2 and the Mad1:C-Mad2 complex should display dynamic properties comparable to those observed in living cells. Ideally, this system might also provide a convincing explanation for the discrepancies in recovery efficiencies in different experiments that we have detailed above. Here we provide an account of our findings.

Results

The binding of Mad2 to the Mad1:Mad2 complex can be visualized by using size-exclusion chromatography (SEC). Recombinant wild-type human Mad2 (Mad2^{wt}) was covalently labeled with Alexa-fluor-488 (abbreviated as Alexa, Figure 1A). When stoichiometric amounts of Alexa-Mad2 and the unlabeled recombinant Mad1:Mad2 complex (whose elution profiles are shown in Figures 1A and 1B, respectively) are mixed, the Alexa-Mad2 signal is incorporated in a high-molecular complex with Mad1:Mad2 (Figure 1C). Identical results were obtained

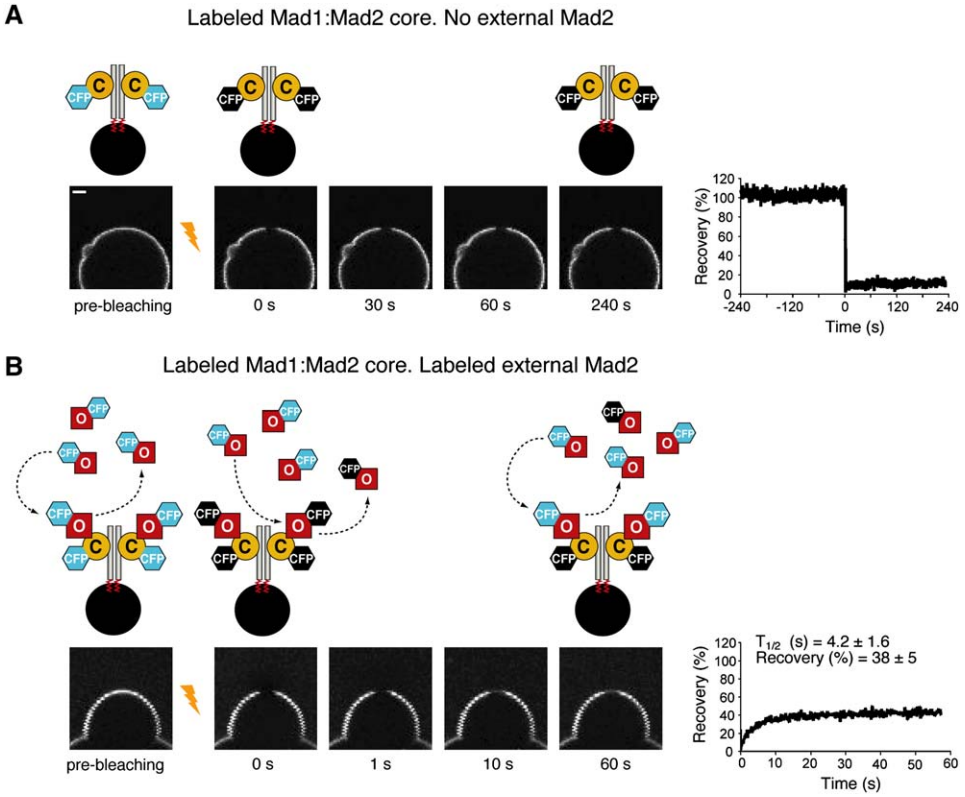

Figure 2. Fluorescence Recovery after Photobleaching of Mad2 In Vitro

(A) Biotin-Mad1:CFP-Mad2 was immobilized on streptavidin beads. CFP-Mad2 fluorescence remained limited to the surface of the beads. There was no significant loss of CFP-Mad2 fluorescence in the prebleaching phase (see graph), indicating that the Mad1:CFP-Mad2 complex does not significantly dissociate and is stably bound to the beads. After bleaching (shown schematically with the appearance of a black CFP hexagon), no recovery is observed. The white bar in the upper left corner of the first panel indicates 10 μm.

(B) As in (A), but with 15 μM CFP-Mad2 added to the medium. After an equilibration phase, bleaching was carried out and recovery monitored. The recovery curve is one of 17 equivalent curves. The statistics on this dataset are described in Table 1F.

if CFP-Mad2 was used instead of Alexa-Mad2 (Figures S1A and S1B in the Supplemental Data available online).

Our recently formulated "Mad2 template" hypothesis [19] suggests that the binding reaction causing the shift of Alexa-Mad2 consists of the binding of O-Mad2 (drafted from the Alexa-labeled population) to a stable C-Mad2 conformer in the Mad1:Mad2 complex (Figure 1D). The hypothesis predicts that the two populations of Mad2 shown in Figure 1D do not exchange subunits, because C-Mad2 does not dissociate from Mad1. Consequently, the "Mad2 template" model predicts that the kinetochore cycle of Mad2 is caused by the binding of O-Mad2 to the C-Mad2 subunits contained in the Mad1:Mad2 complex.

We tested this prediction by using a strategy of in vitro FRAP. For this, we reconstituted a fluorescent version of the Mad1:C-Mad2 kinetochore complex by bacterial coexpression of CFP-Mad2 and biotinylated Mad1 and immobilized it on streptavidin beads. Beads containing Mad1:CFP-Mad2 were brightly fluorescent when imaged with a confocal microscope. Although the complex is noncovalent, fluorescence intensity remained constant in the absence of soluble CFP-Mad2 (Figure 2A). Thus, the Mad1:Mad2 tetramer is sturdy, and the rate of dissociation of CFP-Mad2 from Mad1 is negligible [12, 21]. After CFP bleaching in a small area, no recovery of fluorescence was observed, showing that the immobilized sample does not undergo lateral diffusion at the beads' surface (Figure 2A; see Figures S1 and S2 for additional controls).

Checkpoint response requires both kinetochore-bound and cytosolic Mad2 [17]. To analyze the interaction of "cytosolic" Mad2 with "kinetochores," we added CFP-Mad2 to the medium containing the Mad1:CFP-C-Mad2 beads. In the presence of soluble CFP-Mad2, we observed rapid recovery of 38% ± 5% of the prebleaching fluorescence (Figure 2B and Table 1F). The time-dependency of the recovery was nicely fitted with a single exponential function ($1 - e^{-kt}$) with a recovery half-time ($t_{1/2}$) of 4.2 s. As in living cells [5–8], there is therefore a single type of Mad2 binding site on our in vitro "kinetochores."

Since CFP-C-Mad2 does not dissociate from Mad1 (Figure 2A), the ~40% recovery observed in this experiment must be due to CFP-O-Mad2 cycling between solution and Mad1:C-Mad2. If CFP-O-Mad2 replaced bleached CFP-C-Mad2 directly bound to Mad1, near to full recovery would be predicted. To confirm this, we applied two consecutive rounds of photobleaching to the same area of the beads (Figure 3A and Table 1M). Whereas the first photobleaching was followed by ~40% recovery, the second event resulted in 75% ± 5% recovery, about twice the value observed after the first photobleaching. The half-time of recovery for the

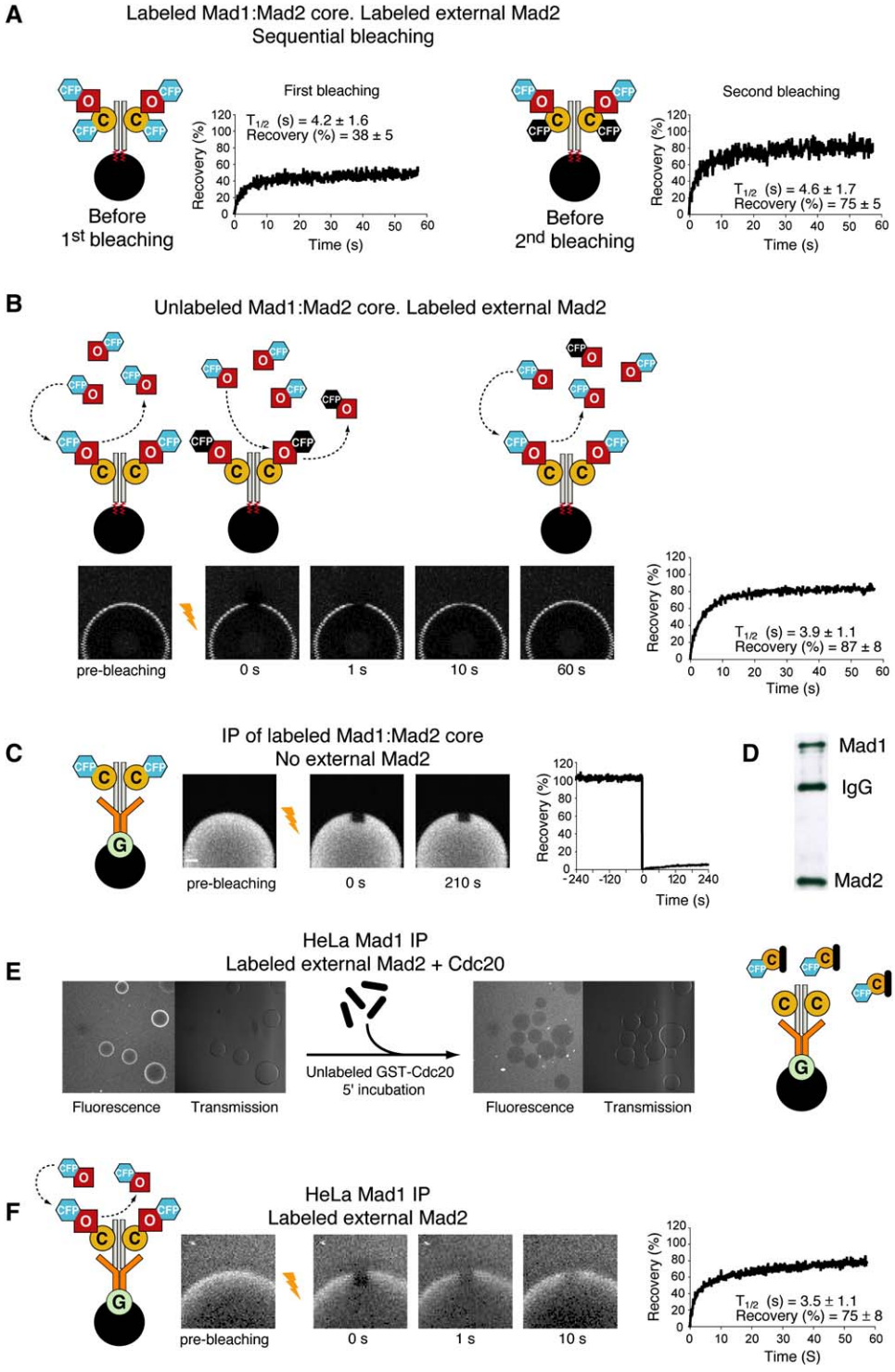

Figure 3. Further Characterization of Mad2 Dynamics In Vitro

(A) Serial photobleaching of CFP-Mad2 in vitro. Two consecutive photobleaching events were imposed on the same area. Recovery after the first photobleaching event is ~38% ± 5%. After the second event, recovery approaches ~75% ± 5%. Statistics for this experiment are in Table 1M.

(B) If C-Mad2 is unlabeled, recovery approaches ~87% ± 8% of the initial fluorescence already after the first bleaching event. See Table 1G for statistics.

(C) Recombinant Mad1:CFP-Mad2 was IPed with an anti-Mad1 monoclonal antibody (shown in orange in the scheme on the left) bound to protein-G on beads (light green circle). There is no significant lateral diffusion of the Mad1:CFP-Mad2 complex on the beads.

(D) Western blotting of Mad1 IP beads from mitotic HeLa-cell extracts with anti Mad1 and anti Mad2 antibodies.

(E) HeLa Mad1 IP beads incubated with 2 μM CFP-Mad2 became brightly fluorescent (left). Addition of $Cdc20^{111–138}$ at 40 μM caused a rapid release of fluorescence from beads (right).

(F) FRAP experiments were carried out with HeLa Mad1 IP beads in the presence of 15 μM CFP-Mad2. Recovery was 75% ± 8% (Table 1H).

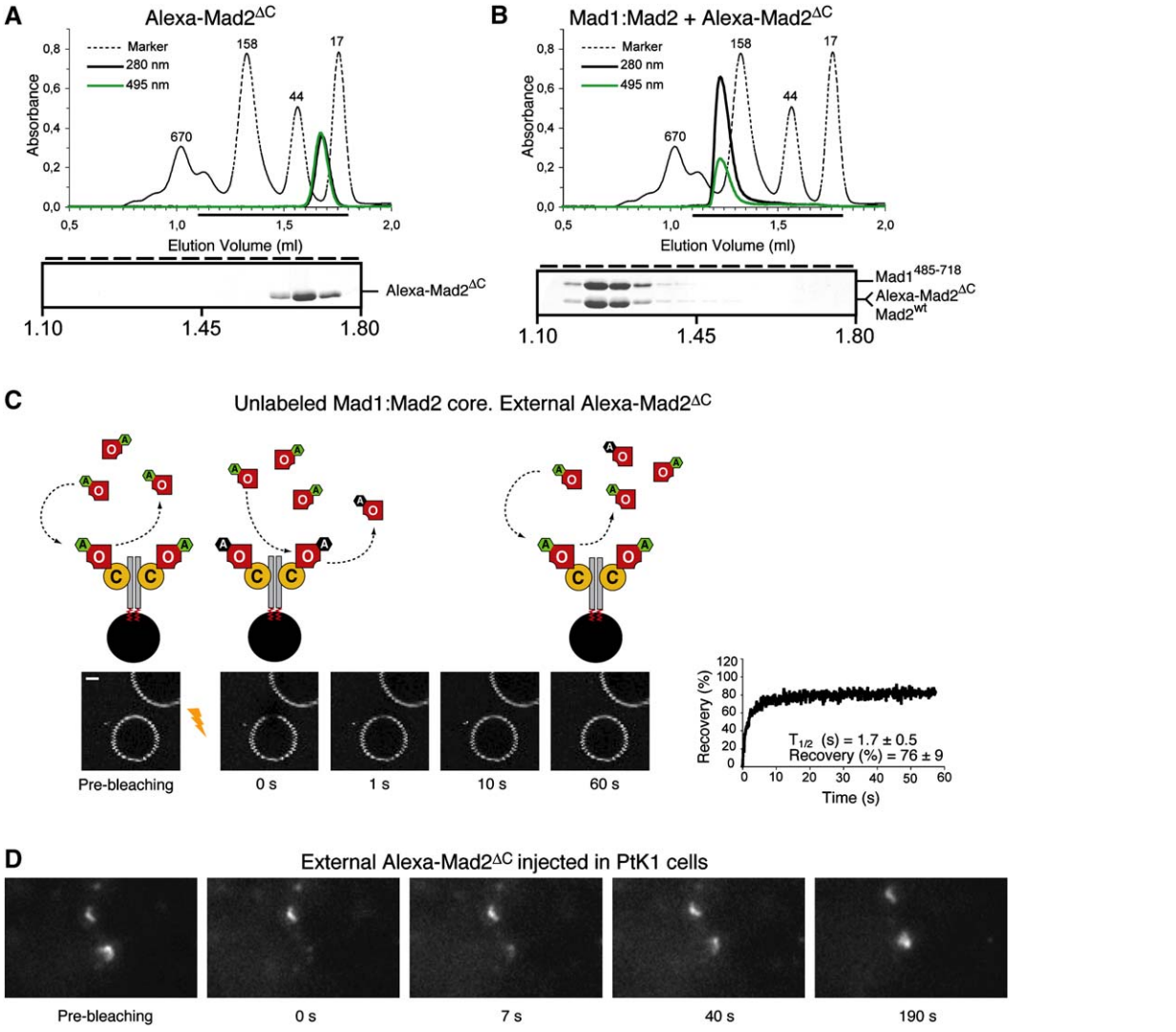

Figure 4. O-Mad2$^{\Delta C}$ Cycles at Kinetochores

(A) Elution profile of Alexa-Mad2$^{\Delta C}$ from a Superdex 200 PC 3.2/30 column.

(B) Alexa-Mad2$^{\Delta C}$ was mixed with stoichiometric amounts of Mad1:Mad2 and incubated for 1 hr. Most Alexa-Mad2$^{\Delta C}$ signal eluted with the Mad1:Mad2 complex, which was shifted toward higher molecular weights upon binding Mad2.

(C) Alexa-Mad2$^{\Delta C}$ was analyzed by FRAP at the surface of beads containing Mad1:C-Mad2.

(D) Alexa-Mad2 was introduced by injection in PtK1 cells and found to localize at kinetochores as described previously [5, 6]. The FRAP experiment shown here reveals that Alexa-Mad2$^{\Delta C}$, like Mad2^{wt}, cycles rapidly at unattached kinetochore in PtK1 cells. Quantification of this experiment is reported in Table 1E.

second event (4.6 s), however, was essentially identical to that of the first event, indicating that recovery is due to the same binding reaction. Thus, the Mad1-bound CFP-C-Mad2 fraction bleached after the first laser pulse cannot be replaced with fluorescent CFP-Mad2. The second FRAP experiment is analogous to carrying out an experiment with beads containing dark biotin-Mad1:C-Mad2 and soluble CFP-Mad2. This experiment resulted in 87% ± 8% fluorescence recovery (Figure 3B and Table 1G). The use of Alexa-Mad2 rather than CFP-Mad2 in the soluble pool did not change significantly the fraction and half-time of recovery (Table 1J).

Next, we asked whether the Mad1:Mad2 complex isolated from HeLa cells is capable of binding fluorescent Mad2 like its recombinant counterpart. For this, we immobilized a monoclonal anti-Mad1 antibody onto protein G-Sepharose beads and immunoprecipitated the Mad1:Mad2 complex from mitotic HeLa cell extracts (see Experimental Procedures). As a positive control, we first carried out an immunoprecipitation (IP) on the recombinant Mad1:CFP-Mad2 complex. Beads bound to the IPed recombinant Mad1:CFP-Mad2 were used in a control FRAP experiment to show that there is no significant lateral diffusion of the fluorescent protein (Figure 3C), presumably because the anti-Mad1 monoclonal antibody binds tightly to Mad1.

Both Mad1 and Mad2 were present in the HeLa IPs (Figure 3D). Upon incubation of the Mad1:Mad2 containing beads with recombinant CFP-Mad2, the beads became fluorescent, indicating that CFP-Mad2 recognizes the precipitated complex (Figure 3E). Binding of CFP-Mad2 to the beads was specific, because the addition

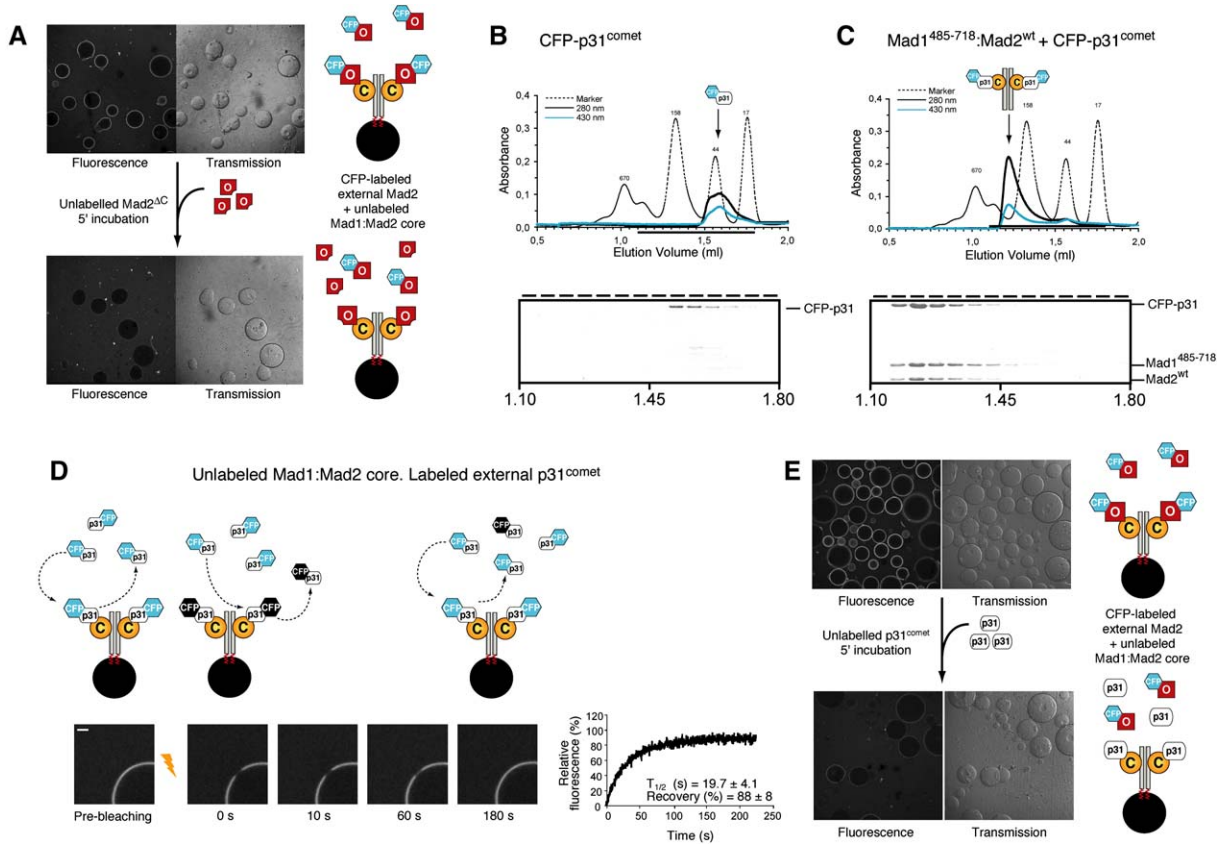

Figure 5. p31^{comet} Interferes with the O-Mad2:C-Mad2 Interaction

(A) Biotin-Mad1:Mad2 was incubated with 15 μM CFP-Mad2^{wt} (upper panel). After equilibration, Mad2$^{\Delta C}$ (30 μM) was added (lower panel). After 5′, most of the CFP-Mad2 fluorescence had dissociated from the beads.

(B) Elution profile of CFP-p31^{comet} from a Superdex 200 PC 3.2/30 SEC column. SDS-PAGE and Coomassie staining of the content of fourteen 50 μl fractions eluting between 1.10 and 1.80 ml. Traces recorded at 280 nm and 458 nm are black and cyan, respectively.

(C) CFP-p31^{comet} and Mad1:C-Mad2 were mixed stoichiometrically and analyzed as above. p31^{comet} was incorporated in the high-molecular-weight complex with Mad1:Mad2.

(D) CFP-p31^{comet} was added to a medium containing biotin-Mad1:Mad2 bound to streptavidin beads. The FRAP behavior of CFP-p31^{comet} is displayed. The dataset is described in Table 1L.

(E) CFP-Mad2 (15 μM) was incubated with biotin-Mad1:Mad2 (upper panel). After equilibration, unlabeled CFP-p31^{comet} was added (15 μM). CFP-Mad2 fluorescence dissociates from the beads (lower panel), indicating that p31^{comet} competes with O-Mad2 for binding C-Mad2.

of synthetic peptide encompassing the Mad2 binding region of Cdc20 (Cdc20$^{111–138}$) caused the dissociation of CFP-Mad2 fluorescence from the beads. This confirms that C-Mad2 created upon binding to Cdc20$^{111–138}$ is unable to bind the C-Mad2 contained in the Mad1:Mad2 IPs. To avoid overinterpretations, however, we wish to clarify that this experiment does not necessarily imply that the binding of O-Mad2 to Cdc20$^{111–138}$ requires, or is facilitated by, the Mad1:Mad2 complex on the beads, because it has been shown before that this interaction advances also in the absence of Mad1:Mad2 in vitro [12, 13, 19]. This issue will be discussed more thoroughly later.

An in vitro FRAP experiment was carried out with Mad1 IPs in the presence of CFP-Mad2 (Figure 3F). Remarkably, the $t_{1/2}$ and percent recovery (3.5 ± 1.1 s and 75% ± 8%, respectively; see Table 1H) were very similar to those measured with the recombinant Mad1:C-Mad2 complex (Table 1G). Overall, these observations are completely consistent with the hypothesis that a stable Mad1:C-Mad2 kinetochore complex accounts for the observed immobile fractions of Mad1 and Mad2 [7, 19].

Table 2. Dissociation Constants

Row	Method	Reaction	K_D	ΔG	ΔH	TΔS	Comments and Reference
A	ITC	O-Mad2 + Mad1-bound C-Mad2	0.95–1.12 μM[a]	−8.1 kcal/mol	−5.5 kcal/mol	2.6 kcal/mol	This study
B	ITC	p31^{comet} + Mad1-bound C-Mad2	25 nM[a]	−10.4 kcal/mol	−11.0 kcal/mol	−0.6 kcal/mol	This study

[a] Two independent measurements gave very similar results. Average values are reported.

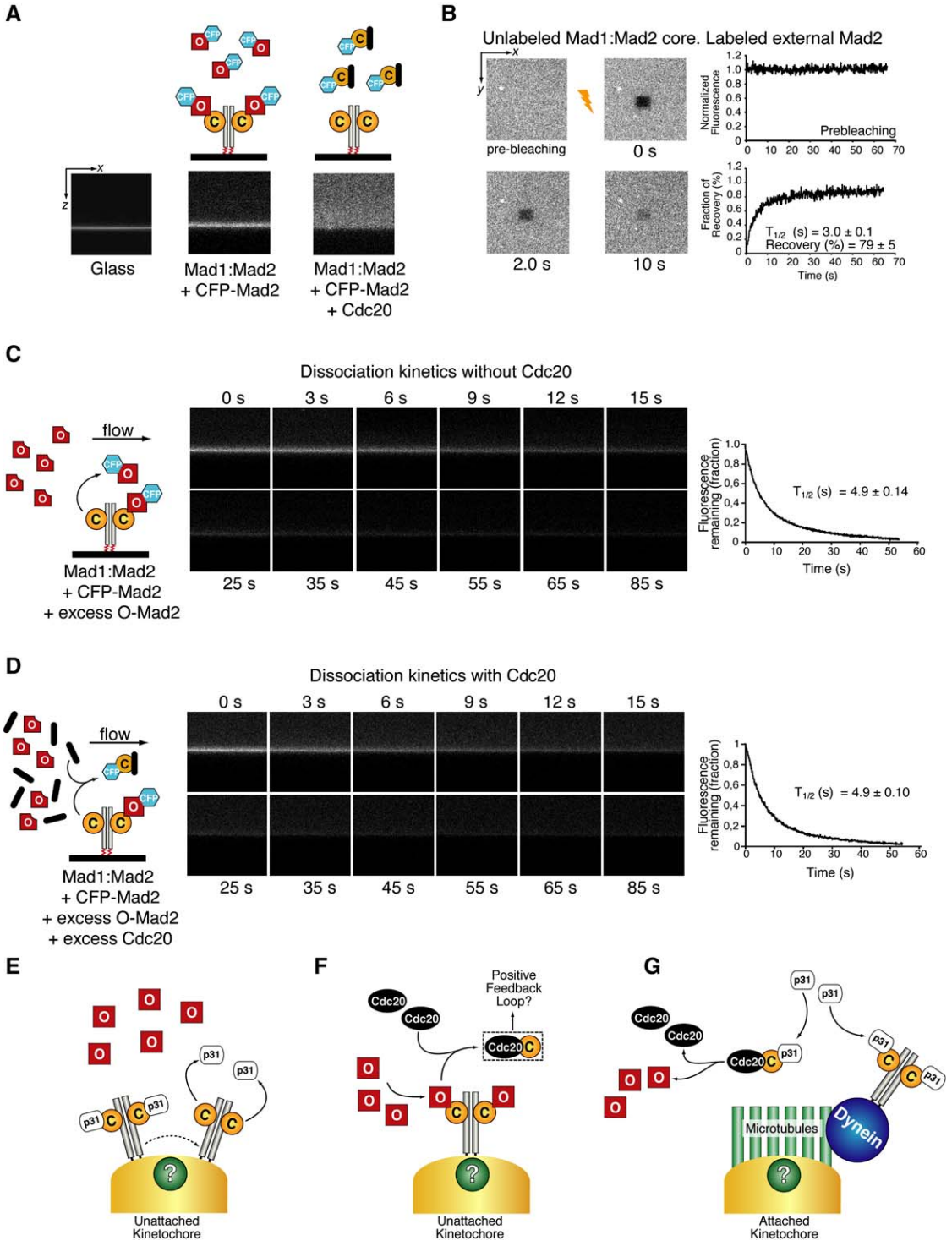

Figure 6. The Dissociation of O-Mad2 from Mad1:C-Mad2 Is Not Affected by Cdc20

(A) Mad1:C-Mad2 was immobilized at the bottom of a 25 μl flow chamber attached to a peristaltic pump. Left panel: the glass surface of the flow chamber. Middle panel: CFP-Mad2 binds the Mad1:C-Mad2 surface. Right panel: the addition of a synthetic peptide corresponding to the Mad2 binding site of Cdc20 (residues 111–138) generates the C-Mad2 version of CFP-Mad2, which is unable to bind the surface.

(B) A FRAP experiment on the flat substrate. Dark Mad1:C-Mad2 and free CFP-Mad2 were used. The experiment is conceptually identical to that shown in Figure 3B. Statistics for this experiment are in Table 1N.

(C) CFP-Mad2 (2 μM) was allowed to equilibrate on the Mad1:C-Mad2 substrate. A solution containing 40 μM O-Mad2$^{\Delta C}$ (or Mad2^{wt}, Table 1O) was flowed in the chamber and the dissociation of CFP-Mad2 monitored. The dissociation rates in the presence of 40 μM dark Mad2^{wt} were essentially identical (data not shown). The dataset is described in Table 1P.

(D) The same reaction using all of the above and 40 μM Cdc20$^{111–138}$ peptide. The dataset is described in Table 1Q. Mad2$^{\Delta C}$ was used as dark O-Mad2 in this experiment because this mutant binds Mad1:C-Mad2 but is unable to bind Cdc20, and therefore will not deplete Cdc20 in solution [19].

This complex, in turn, appears to be responsible for the recruitment of a mobile fraction of O-Mad2 from the cytosol. We suspect that the ~10%–20% deviation of the observed recovery values from the expected values in different experiments (see Table 1) is caused by photodamage of the receptor-ligand complexes by the high laser power required for photobleaching. We are presently exploring strategies to limit this effect.

Mad2$^{\Delta C}$ is a Mad2 deletion mutant stably locked in the O-Mad2 conformation and unable to bind Mad1 or Cdc20 [19]. Previously, we have shown that this mutant is able to localize to the kinetochore upon injection in PtK1 cells [19]. In agreement with the hypothesis that the Mad1:Mad2 complex is responsible for the recruitment of Mad2$^{\Delta C}$ to kinetochores, Alexa-Mad2$^{\Delta C}$ bound the recombinant Mad1:Mad2 complex indistinguishably from Alexa-Mad2^{wt} (Figures 4A–4B). Because Mad2$^{\Delta C}$ is unable to bind Mad1, this result shows that the binding of O-Mad2 to the Mad1:Mad2 complex does not imply direct binding to Mad1.

Mad2$^{\Delta C}$ cycled on the recombinant Mad1:Mad2 complex with slightly faster dynamics relative to Mad2^{wt} (Figure 4C and Table 1J and 1K), possibly reflecting a marginal contribution of the O-Mad2 C-terminal tail, which is partly deleted in Mad2$^{\Delta C}$, to formation of the O-Mad2:C-Mad2 complex. Consistent with these results in vitro, Alexa-Mad2$^{\Delta C}$ introduced in mitotic PtK1 cells by microinjection cycled at kinetochores with kinetics that were similar to those previously observed when Mad2^{wt} was used in vivo [5, 6], but, as for the in vitro case, were slightly faster relative to Mad2^{wt} (Figure 4D and Table 1E).

The overexpression of Mad2$^{\Delta C}$ has a dominant-negative effect on the SAC [19, 20, 22, 23]. This effect is likely due to the fact that Mad2$^{\Delta C}$ binds C-Mad2 and competitively inhibits binding of O-Mad2^{wt}, preventing Mad2^{wt} from reaching Cdc20. To illustrate this, we bound CFP-Mad2 to immobilized Mad1:C-Mad2 (Figure 5A, upper panel). We then added a 2-fold excess of unlabeled Mad2$^{\Delta C}$. This readily displaced CFP-Mad2 from the beads (Figure 5A, lower panel).

Unlike Mad2$^{\Delta C}$, which deregulates the SAC nonphysiologically, the Mad2 binding protein p31^{comet} (previously CMT2) is a physiological negative regulator of the SAC [24, 25]. The observation that p31^{comet} binds selectively to C-Mad2 and does not bind O-Mad2 prompted the suggestion that p31^{comet} might prevent C-Mad2 from sequestering Cdc20 [25]. In contradiction to this expectation, however, p31^{comet} was found to bind tightly to the Cdc20:C-Mad2 complex without affecting its stability [25], so p31^{comet} must function in a different way.

Because C-Mad2 is present both in the Mad1:C-Mad2 and in the Cdc20:C-Mad2 complexes, p31^{comet}, which has been previously shown to bind Cdc20:C-Mad2 [25], is also predicted to bind Mad1:C-Mad2. Indeed, CFP-p31^{comet} formed a tight complex with Mad1:C-Mad2 (Figures 5B and 5C), whose dissociation constant (K_D) by ITC was ~25 nM (Table 2B). In agreement with its tight binding, CFP-p31^{comet} cycled on the Mad1:C-Mad2 complex with a half-time of recovery of 20 s, indicative of a slower rate of dissociation relative to ~4 s half-life of Mad2. The percent recovery was ~90% (Figure 5D and Table 1L).

The Mad2 template model [19, 26–28] suggests an alternative hypothesis for understanding the function of p31^{comet}. The model proposes that the interaction between O-Mad2 and C-Mad2 activates O-Mad2 for Cdc20 binding and is therefore critical for the SAC. Interfering with this interaction will depress the SAC, as illustrated by the dominant-negative effects of Mad2$^{\Delta C}$. Thus, we asked whether binding of p31^{comet} to C-Mad2 might interfere with the binding of O-Mad2, as is the case for Mad2$^{\Delta C}$. Beads containing immobilized Mad1:C-Mad2 became brightly fluorescent in a medium containing CFP-Mad2 (Figure 5E, upper panel). Shortly after the addition of an equimolar amount of unlabeled p31^{comet}, the fluorescence of CFP-Mad2 became almost entirely displaced from the beads (Figure 5E, lower panel), showing that p31^{comet} binds C-Mad2 competitively with O-Mad2. Thus, the effects of p31^{comet} are essentially identical to those observed with Mad2$^{\Delta C}$, whose expression abrogates the SAC.

Cdc20 cycles rapidly at kinetochores [5–8]. Whether this cycle reflects its capture by Mad2 is currently unclear. Conversely, it is unknown whether the Mad2 cycle on kinetochores is influenced by Cdc20, the protein to which Mad2 is expected to bind at kinetochores. In this respect, it is interesting to note that Mad2$^{\Delta C}$, which does not bind Cdc20 [19, 21], cycled on C-Mad2 in vitro and in vivo with a turnover rate similar to that of Mad2^{wt} (Table 1D, 1E, 1J, and 1K and Figure 4). This implies that Cdc20 does not influence the turnover rate of kinetochore Mad2, suggesting that Mad2 is released from kinetochores before it binds Cdc20. An alternative explanation, however, is that only a small fraction of O-Mad2 cycling on Mad1:C-Mad2 at kinetochores is removed by Cdc20, too small to be observed in the Mad2 FRAP curves in vivo.

To shed light on this issue, we developed an implementation of our recruitment assay allowing continuous imaging of a surface containing immobilized Mad1:C-Mad2 while being perfused with a solute. Biotinylated nonfluorescent Mad1:C-Mad2 was immobilized on the bottom surface of a flow cell connected to a peristaltic pump. CFP-Mad2 was injected, and the flow was stopped to allow equilibration. CFP-Mad2 bound readily to the surface containing the Mad1:C-Mad2 receptor. If

(E) We speculate that the recruitment of the Mad1:C-Mad2 complex to an unattached kinetochore results in the inactivation of p31^{comet} and its fast release from kinetochores. Note that p31^{comet} may undergo a continuous cycle of inactivation at unattached kinetochores similar to the Mad2 activation cycle. An unknown kinetochore function (green ball with question mark) inactivates p31^{comet}.

(F) Cytosolic Mad2 has the O-Mad2 conformation [19, 20]. The Mad1:C-Mad2 complex recruits O-Mad2 to kinetochores, and O-Mad2 is converted into C-Mad2 bound to Cdc20. Mad2:Cdc20 is a structural copy of Mad1:Mad2, because Mad1 and Cdc20 share a Mad2 binding motif, and Mad2 adopts the same C-Mad2 conformation in these complexes. The "Mad2 template" model [19] predicts that C-Mad2:Cdc20 is a structural equivalent of Mad1:Mad2 and converts more O-Mad2 into Cdc20-bound C-Mad2, possibly creating a positive feedback module for amplification of the SAC signal.

(G) After microtubule attachment, Dynein removes Mad1:C-Mad2 from kinetochores [10]. Mad1:Mad2 is thus separated from the kinetochore function that inactivates p31^{comet}. This eventually leads to the reactivation of p31^{comet}, which acts as a "screen" that interposes itself.

the same experiment was carried out in the presence of the Cdc20$^{111–138}$ synthetic peptide, CFP-Mad2 did not accumulate on the surface, confirming that binding is specific for O-Mad2 (Figure 6A). To assess the dynamic properties of Mad2 in this new system, we performed a FRAP experiment similar to that shown in Figure 3B. The half-time and fraction of recovery were very similar to those obtained on beads (Figure 6B and Table 1N).

To assess whether Cdc20 accelerates the removal of O-Mad2 from the Mad1:C-Mad2 complex, we carried out an "off rate" experiment (Figure 6C). CFP-Mad2 (2 μM) was equilibrated on the immobilized Mad1:Mad2 complex. We monitored the dissociation of CFP-Mad2 from the Mad1:C-Mad2 surface while injecting into the chamber a solution containing a 20-fold excess of dark O-Mad2$^{\Delta C}$ (which binds C-Mad2; identical results were obtained with dark Mad2^{wt}, data not shown) to prevent CFP-Mad2 re binding to Mad1:Mad2. A plot of the time course of dissociation of CFP-Mad2 from Mad1:Mad2 displayed a single exponential decay with a half-time of 4.9 s, slightly longer than but in very good agreement with the values determined by FRAP (Figure 6C, data not shown, and Table 1O and 1P). Next, we repeated this experiment after adding Cdc20 (at 40 μM) together with the same excess of dark O-Mad2$^{\Delta C}$. The dissociation curve was fitted with a single exponential function with a half-time of dissociation essentially identical to that measured in the absence of Cdc20 (Figure 6D and Table 1Q). These results indicate that Cdc20 does not influence the turnover of kinetochore Mad2, at least in the absence of a Cdc20 binding site near the Mad1:C-Mad2 complex.

Discussion

Our in vitro FRAP analysis recapitulates faithfully the results of previous FRAP analyses of Mad2 carried out in living cells [5–7]. The analysis provides a straightforward explanation of the differences in percent recoveries between experiments in which transient expression or protein injection of fluorescent Mad2 was used, reporting near to full recovery of kinetochore Mad2 fluorescence [5, 6], as opposed to experiments using stable YFP-Mad2 expression and reporting 50% recovery [7]. The most likely explanation of these discrepancies is that the stability of the Mad1:C-Mad2 complex prevents the binding of the fluorescent Mad2 species to Mad1, unless a long-term expression strategy is adopted, as was the case for the experiments using stable YFP-Mad2 cell lines. This interpretation is confirmed by the fact that the percent recovery of Alexa-Mad2$^{\Delta C}$ injected into PtK1 cells is also near 100% (Figure 4 and Table 1E), as it is for Alexa-Mad2^{wt} [5, 6]. Because Mad2$^{\Delta C}$ is unable to bind Mad1 whereas Mad2^{wt} is in principle able to do it, the fact that both constructs provide the same fraction of recovery suggests that there is not enough time for fluorescent Mad2^{wt} to bind Mad1 in these experiments. Consistent with this prediction, if the FRAP experiment in vitro was carried out with unlabeled Mad1:Mad2 complex, near to 90% recovery was observed (Figure 3B and Table 1G). This underscores the accuracy with which in vitro FRAP might provide detailed molecular accounts of dynamic live-cell measurements.

So far, the studies in living cells have reported somewhat different half-times of recovery, ranging between 6 and 25 s (Table 1A–1D). Different camera acquisition rates, sensitivities, and phototoxicity might all affect the initial part of the recovery curve and provide somewhat different accounts of the times of recovery. In vitro, we have consistently measured a half-time of ~3–5 s for the Mad2 cycle (Table 1). This value is not more dissimilar from the in vivo data than the in vivo measurements among themselves. At present, we are unable to provide a certain explanation for the observed discrepancy. We note that it is possible that the slightly faster half-times observed in vitro might reflect modulations of the affinity of the interaction of the Mad1:C-Mad2 receptor for O-Mad2 in vivo. In particular, a decreased half-time (that is, a faster k_{off}) implies (assuming an identical k_{on}) a decrease in the affinity of the interaction. It is possible that additional interactions, such as for instance additional van der Waals contacts or additional hydrogen bonds, provide an increased binding energy to the interaction. If existing, however, these effects must be minimal because a 2- to 5-fold change in k_{off} would only predict a linear 2- to 5-fold change in the K_D of the interaction. We also note that in cellular FRAP experiments carried out so far, the fluorescent species coexisted with endogenous nonfluorescent molecules. Thus, dark endogenous molecules might compete with fluorescent ones so that the apparent recovery will appear slower than it would be in the absence of dark competitors.

Our results show unequivocally that the Mad1:C-Mad2 complex does not dissociate during mitosis [7, 19]. The implication of this is that the two pools of Mad2, the C-Mad2 pool bound to Mad1 and the cytosolic O-Mad2 pool destined to Cdc20, are distinct and nonexchanging. Furthermore, this implies that the molecules of Mad2 eventually destined to bind Cdc20 are drafted exclusively from the cytosolic pool. The interaction of these two genetically identical but conformationally dissimilar pools in the O-Mad2:C-Mad2 complex is a striking characterizing element of the Mad2 checkpoint and bears clear resemblances—in addition to important differences—with prion proteins [29].

Our experiments also suggest that Cdc20 does not influence the rate of dissociation of "external" Mad2 from its complex with Mad1:C-Mad2 (Figure 6). A possible caveat with these experiments is that they were carried out with a short segment of Cdc20, and we cannot exclude that the missing segments of Cdc20 are important to accelerate the dissociation of Mad2 from the Mad1:Mad2 complex. Future mechanistic studies on how the interaction of O-Mad2 with C-Mad2 fosters the interaction with Cdc20 will have to address the actual conformation of Mad2 dissociating from Mad1:Mad2. For this, we envision that a real-time sensor of Mad2 conformation will need to be developed.

Although Mad2 is able to bind Cdc20 in vitro in the absence of other proteins, the interaction is slow. For instance, the binding of O-Mad2 to a synthetic peptide encompassing the Cdc20 sequence has an association rate (k_{on}) in the range of 10^2 $M^{-1}s^{-1}$ (M.V. and A.M., unpublished data). A slow rate of association is expected if one considers the extent of the conformational change O-Mad2 needs to undergo to bind Cdc20 turning into C-Mad2. We suspect that the significance of the interaction of O-Mad2 with C-Mad2 is to accelerate this structural conversion, possibly explaining the catalytic role

played by unattached kinetochores (i.e., Mad1:C-Mad2) in generating the checkpoint signal.

It is also intriguing that the intrinsic properties of the interaction between the two pools of Mad2 and its regulation by $p31^{comet}$ appear to be largely sufficient for explaining the kinetochore cycle of Mad2. Our results delineate a model predicting that kinetochores cause the inactivation of $p31^{comet}$ and its release from Mad1:C-Mad2 to allow kinetochore recruitment of O-Mad2 (Figures 6E–6G). The latter might be modified at kinetochores and released in an activated form that binds rapidly to Cdc20. Microtubule attachment results in the depletion of Mad1 and Mad2 from kinetochores [10], and this may coincide with the reactivation of $p31^{comet}$ and subsequent inhibition of the O-Mad2:C-Mad2 interaction. The "Mad2 template" model predicts a direct catalytic role of C-Mad2 on the transformation of O-Mad2 to C-Mad2 bound to Cdc20. Testing this prediction is clearly essential for validating the model.

Conclusions

A proper understanding of the molecular network responsible for the spindle checkpoint requires a systems approach, based upon law of mass action and mathematical modeling [3, 4]. Oftentimes kinetic models are underdetermined because experimental values for rate constants and concentration are lacking. In vitro FRAP and the other approaches reported here can contribute to solving this major shortcoming of the modeling approach. In particular, we show in Supplemental Experimental Procedures that combining in vitro FRAP with a measure of K_D allows the estimation of both kinetic parameters (k_{on} and k_{off}) of an interaction. The procedure is completely general and may be extended to the study of virtually any macromolecular interaction.

Experimental Procedures

Protein Expression, Covalent Modifications of Proteins, and Immunoprecipitations

Readers are referred to the Supplemental Experimental Procedures section in the Supplemental Data.

In Vitro FRAP, Beads Implementation

Agarose beads with immobilized streptavidin (SIGMA, S1638) were washed and equilibrated in PBS. Purified biotin-Mad1:CFP-Mad2 or biotin-Mad1:Mad2 were added at streptavidn:biotin ratio of ~32:1 and incubated for 1 hr at 4ºC. Beads with immobilized Mad1:Mad2 were washed with PBS and stored at −80ºC until use. FRAP measurements were performed on a Leica TCS SP2 confocal microscope equipped with a 63×/1.40 (OIL CS HC×PL APO) objective lens (Leica). Streptavidin-agarose beads containing ~10 pmoles of immobilized Mad1/Mad2 core complexes were typically mixed in a chambered coverglass well (Lab-Tek II) with 1500 pmoles external ligand (Mad2 or $p31^{comet}$) in a final volume of 100 μl PBS, yielding molar concentrations of 0.1 μM and 15 μM, respectively. External ligand concentrations of 15 μM and above were found to saturate kinetics and to yield reproducible results. Imaging was controlled by Leica Confocal Software (v. 2.61), and photobleaching was carried out with the 488 nm line (Alexa-488) and the 458 nm line (CFP) of an Ar/ArKr laser at 20 mW. An area with an approximate diameter of 10 μm at the edge of a bead was bleached, and images were collected with a temporal resolution of 115 ms between frames. ImageJ software was used to calculate mean pixel intensities of bleached areas with time, and the values were exported to an Excel spreadsheet. Recovery percentage was taken as the final average plateau intensity (F_∞) minus the fluorescence immediately after photobleaching (F_0), all divided by the difference between prebleach (F_I) and postbleach intensities $[(F_\infty - F_0)/(F_I - F_0)]$. The exponential kinetics of FRAP was analyzed by calculating the normalized unrecovered fluorescence at each time-point $[(F_\infty - F_t)/(F_\infty - F_0)]$. Recovery half-times ($t_{1/2}$) were calculated according to $t_{1/2} = \ln(2)/k$, where k is the time constant for a single-exponential recovery model [30]. For ensuring possible artifact of photobleaching, the mean pixel intensities of the areas on the beads surrounding the bleached area were monitored. If photobleaching occurred (<95% of original value at the end of the experiment), or if the bead moved during analysis, that particular measurement was excluded. All recovery measurements displayed single exponential recovery kinetics.

In Vitro FRAP, Flat Surface

Twenty-five microliters flow cells (μ-slide VI Flow-trough, Ibidi GmbH, Munich, Germany) were coated with streptavidin essentially as described [31]. The flow cell was injected with the following reagents in subsequent steps: 30 μl of 2.5 mg/ml Biotin-BSA (Pierce, ImmunoPure Biotin-LC-BSA, #29130) dissolved in MilliQ water, 30 μl 1 mg/ml NeutrAvidin (Molecular Probes, A-2666) in TRIS-EDTA buffer, and 30 μl 5 mg/ml BSA (A-9085 Sigma) in MilliQ water. Each incubation was protracted for 30 min. After a washing step with MilliQ water (5× chamber volume), the flow cell was equilibrated with PBS. After this, 30 μl of 1 μM purified biotin-Mad1:Mad2 complex in PBS was added and incubated for 30 min. Finally, the cells were washed with 125 μl PBS. In vitro FRAP experiments were performed with 2 μM external CFP-Mad2 equilibrated with immobilized biotin-Mad1:Mad2. Photobleaching, data acquisition, and analysis were performed as described above for the beads assay.

In Vivo FRAP

FRAP experiments on kinetochore-bound Alexa-$Mad2^{\Delta C}$ and Alexa-$Mad2^{wt}$ in PtK1 cells were carried out precisely as described before [5, 6]. The quantification of these experiments is reported in Table 1.

Dissociation Rates

Imaging of dissociation experiments was carried out with a temporal resolution of 0.15 s. The reaction was first driven to equilibration by using 2 μM CFP-Mad2 on the immobilized biotin-Mad1:Mad2. Dissociation was filmed while 50 μl of a 40-fold excess of O-Mad2 was injected at a flow rate of 25 μl/s. The images were analyzed with ImageJ software, and the data were exported to an Excel spreadsheet for analysis.

Relation of the FRAP Recovery-Rate Constant to k_{off} and Estimation of k_{on}

Readers are referred to the Supplemental Experimental Procedures in the Supplemental Data.

Supplemental Data

Supplemental Data include Supplemental Experimental Procedures and two figures and are available with this article online at: http://www.current-biology.com/cgi/content/full/16/8/755/DC1/.

Acknowledgements

AM is grateful to Italian Association for Cancer Research, Human Frontier Science Program, EU FP6 programs 3D-Repertoire and Mitocheck, Fondazione Telethon, Fondo FIRB and Fondazione Cariplo for generous funding. ADA is a former EMBO long-term postdoctoral fellow and a postdoctoral fellow of the Italian Foundation for Cancer Research.

Received: January 27, 2006
Revised: March 5, 2006
Accepted: March 7, 2006
Published: April 17, 2006

References

1. Carrero, G., McDonald, D., Crawford, E., de Vries, G., and Hendzel, M.J. (2003). Using FRAP and mathematical modeling to determine the in vivo kinetics of nuclear proteins. Methods *29*, 14–28.

2. Sprague, B.L., and McNally, J.G. (2005). FRAP analysis of binding: Proper and fitting. Trends Cell Biol. *15*, 84–91.
3. Kirschner, M.W. (2005). The meaning of systems biology. Cell *121*, 503–504.
4. Tyson, J.J., Chen, K.C., and Novak, B. (2003). Sniffers, buzzers, toggles and blinkers: Dynamics of regulatory and signaling pathways in the cell. Curr. Opin. Cell Biol. *15*, 221–231.
5. Howell, B.J., Moree, B., Farrar, E.M., Stewart, S., Fang, G., and Salmon, E.D. (2004). Spindle checkpoint protein dynamics at kinetochores in living cells. Curr. Biol. *14*, 953–964.
6. Howell, B.J., Hoffman, D.B., Fang, G., Murray, A.W., and Salmon, E.D. (2000). Visualization of Mad2 dynamics at kinetochores, along spindle fibers, and at spindle poles in living cells. J. Cell Biol. *150*, 1233–1250.
7. Shah, J.V., Botvinick, E., Bonday, Z., Furnari, F., Berns, M., and Cleveland, D.W. (2004). Dynamics of centromere and kinetochore proteins; implications for checkpoint signaling and silencing. Curr. Biol. *14*, 942–952.
8. Kallio, M.J., Beardmore, V.A., Weinstein, J., and Gorbsky, G.J. (2002). Rapid microtubule-independent dynamics of Cdc20 at kinetochores and centrosomes in mammalian cells. J. Cell Biol. *158*, 841–847.
9. Cleveland, D.W., Mao, Y., and Sullivan, K.F. (2003). Centromeres and kinetochores: From epigenetics to mitotic checkpoint signaling. Cell *112*, 407–421.
10. Musacchio, A., and Hardwick, K.G. (2002). The spindle checkpoint: Structural insights into dynamic signalling. Nat. Rev. Mol. Cell Biol. *3*, 731–741.
11. Bharadwaj, R., and Yu, H. (2004). The spindle checkpoint, aneuploidy, and cancer. Oncogene *23*, 2016–2027.
12. Sironi, L., Mapelli, M., Knapp, S., Antoni, A.D., Jeang, K.-T., and Musacchio, A. (2002). Crystal structure of the tetrameric Mad1-Mad2 core complex: Implications of a 'safety belt' binding mechanism for the spindle checkpoint. EMBO J. *21*, 2496–2506.
13. Luo, X., Tang, Z., Rizo, J., and Yu, H. (2002). The Mad2 spindle checkpoint protein undergoes similar major conformational changes upon binding to either Mad1 or Cdc20. Mol. Cell *9*, 59–71.
14. Fraschini, R., Beretta, A., Sironi, L., Musacchio, A., Lucchini, G., and Piatti, S. (2001). Bub3 interaction with Mad2, Mad3 and Cdc20 is mediated by WD40 repeats and does not require intact kinetochores. EMBO J. *20*, 6648–6659.
15. Hwang, L.H., Lau, L.F., Smith, D.L., Mistrot, C.A., Hardwick, K.G., Hwang, E.S., Amon, A., and Murray, A.W. (1998). Budding yeast Cdc20: A target of the spindle checkpoint. Science *279*, 1041–1044.
16. Martin-Lluesma, S., Stucke, V.M., and Nigg, E.A. (2002). Role of hec1 in spindle checkpoint signaling and kinetochore recruitment of mad1/mad2. Science *297*, 2267–2270.
17. Chung, E., and Chen, R.-H. (2002). Spindle checkpoint requires Mad1-bound and Mad1-free Mad2. Mol. Biol. Cell *13*, 1501–1511.
18. Chen, R.H., Brady, D.M., Smith, D., Murray, A.W., and Hardwick, K.G. (1999). The spindle checkpoint of budding yeast depends on a tight complex between the Mad1 and Mad2 proteins. Mol. Biol. Cell *10*, 2607–2618.
19. De Antoni, A., Pearson, C.G., Cimini, D., Canman, J.C., Sala, V., Nezi, L., Mapelli, M., Sironi, L., Faretta, M., Salmon, E.D., et al. (2005). The mad1/mad2 complex as a template for mad2 activation in the spindle assembly checkpoint. Curr. Biol. *15*, 214–225.
20. Luo, X., Tang, Z., Xia, G., Wassmann, K., Matsumoto, T., Rizo, J., and Yu, H. (2004). The Mad2 spindle checkpoint protein has two distinct natively folded states. Nat. Struct. Mol. Biol. *11*, 338–345.
21. Sironi, L., Melixetian, M., Faretta, M., Prosperini, E., Helin, K., and Musacchio, A. (2001). Mad2 binding to Mad1 and Cdc20, rather than oligomerization, is required for the spindle checkpoint. EMBO J. *20*, 6371–6382.
22. Canman, J.C., Salmon, E.D., and Fang, G. (2002). Inducing precocious anaphase in cultured mammalian cells. Cell Motil. Cytoskeleton *52*, 61–65.
23. Mikhailov, A., Cole, R.W., and Rieder, C.L. (2002). DNA damage during mitosis in human cells delays the metaphase/anaphase transition via the spindle-assembly checkpoint. Curr. Biol. *12*, 1797–1806.
24. Habu, T., Kim, S.H., Weinstein, J., and Matsumoto, T. (2002). Identification of a MAD2-binding protein, CMT2, and its role in mitosis. EMBO J. *21*, 6419–6428.
25. Xia, G., Luo, X., Habu, T., Rizo, J., Matsumoto, T., and Yu, H. (2004). Conformation-specific binding of p31(comet) antagonizes the function of Mad2 in the spindle checkpoint. EMBO J. *23*, 3133–3143.
26. Nasmyth, K. (2005). How do so few control so many? Cell *120*, 739–746.
27. Hagan, R.S., and Sorger, P.K. (2005). Cell biology: The more MAD, the merrier. Nature *434*, 575–577.
28. Hardwick, K.G. (2005). Checkpoint signalling: Mad2 conformers and signal propagation. Curr. Biol. *15*, R122–R124.
29. Chan, G.K., Liu, S.T., and Yen, T.J. (2005). Kinetochore structure and function. Trends Cell Biol. *15*, 589–598.
30. Bulinski, J.C., Odde, D.J., Howell, B.J., Salmon, T.D., and Waterman-Storer, C.M. (2001). Rapid dynamics of the microtubule binding of ensconsin in vivo. J. Cell Sci. *114*, 3885–3897.
31. Yildiz, A., Forkey, J.N., McKinney, S.A., Ha, T., Goldman, Y.E., and Selvin, P.R. (2003). Myosin V walks hand-over-hand: Single fluorophore imaging with 1.5-nm localization. Science *300*, 2061–2065.